SAND2000-1644J

# Magnetoconductance of independently tunable tunnel-coupled double quantum wires

M. A. Blount[1,2], J. S. Moon[1], J. A. Simmons[1,2], S. K. Lyo[1], J. R. Wendt[1], J. L. Reno[1]
[1]*Sandia National Laboratories, Albuquerque, New Mexico, 87185, USA*
[2]*University of New Mexico, Department of Physics and Astronomy, NM 87131, USA*

We report on our recent experimental studies of vertically-coupled quantum point contacts subject to in-plane magnetic fields. Using a novel flip-chip technique, mutually aligned split gates on both sides of a sub micron thick double quantum well heterostructure define a closely-coupled pair of ballistic one-dimensional (1D) constrictions. We observe quantized conductance steps due to each quantum well and demonstrate independent control of each 1D constriction width. In addition, a novel magnetoconductance feature at ~6 T is observed when a magnetic field is applied perpendicular to both the current and growth directions. This conductance dip is observed only when 1D subbands are populated in both the top and bottom constrictions. This data is consistent with a counting model whereby the number of subbands crossing the Fermi level changes with field due to the formation of an anticrossing in each pair of 1D subbands.

Coupled low dimensional electronic systems have become of increasing interest recently due to advances in fabrication technology. While much attention has been focused on closely coupled two-dimensional electron systems and coupled quantum dots, little work has been done on coupled quantum wires. Early work focused on tunneling between wires defined laterally by planar lithography, in which case the lateral tunneling is weak and the barrier profile poorly characterized. [1] Recently, vertically coupled quantum wires were fabricated in a double quantum well (DQW) heterostructure by mesa etching. [2] This system has a narrow tunnel barrier, yet lacks the control over constriction width that split gates can provide.

To overcome these difficulties, we have fabricated a pair of vertically coupled quantum point contacts (VCQPCs) using mutually aligned top and back split gates in a closely coupled GaAs/$Al_{0.3}Ga_{0.7}As$ DQW. The DQW had 200 Å wells separated by an 11 Å barrier. The two occupied subbands of the DQW had densities of 2.5 and 1.2 x $10^{11}$ $cm^{-2}$, and had a total mobility of 5.8 x $10^5$ $cm^2/Vs$, yielding a mean free path of ~10 μm. A symmetric-antisymmetric energy gap $\Delta_{SAS}$ = 1.7 meV was measured, corresponding to the minimum density difference between the two lowest energy subbands when the QWs are balanced. We used the epoxy-bond-and-stop-etch (EBASE) technique, described elsewhere [3], to define a pair of vertically aligned split

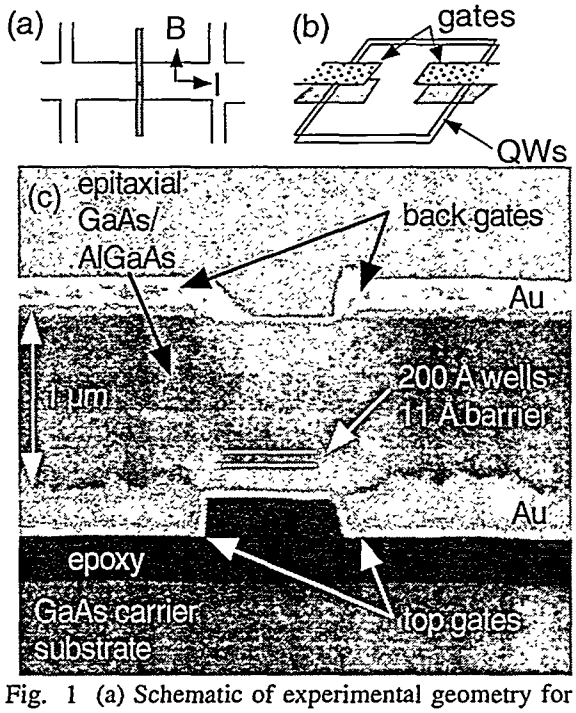


Fig. 1 (a) Schematic of experimental geometry for magnetoconductance measurement. (b) Split gate geometry. (c) Scanning electron micrograph of a test structure. The actual sample was only 3000 Å thick, so that the front and back split gates were equally distant from the electron layers.

## DISCLAIMER

## DISCLAIMER

**Portions of this document may be illegible in electronic image products. Images are produced from the best available original document.**

gates by electron beam lithography *on each side* of the DQW heterostructure, whose thickness is only 3000 Å. Not only does this process allow sub-tenth-micron alignment of top and back gates, but has no deleterious effect on sample mobility. The resulting sample has both top and back split gates, each placed only ~1500 Å from the DQW. Fig. 1(a) and (b) show schematics of the sample, and Fig. 1(c) shows a scanning electron micrograph of a cross sectioned dual split-gate test structure of similar geometry, but a thickness of ~1 μm.

By controlling the relative values of top and back split-gate voltages $V_T$ and $V_B$, the sample can be tuned into five different regimes depending on the widths of the individual QWs. These regimes are (i) 2D-2D; (ii) 2D-1D; (iii) 1D-1D; (iv) 1D-pinched-off; and (v) both pinched-off. Fig. 2 shows the sample resistance as a function of $V_T$, with $V_B = 0$. A number of features appear which correspond to transitions between the different regimes. At $V_T = 0$, both channels are 2D. As $V_T$ is made increasingly negative, the channel resistance shows a clear shoulder at –0.3 V followed by a sharp increase at –0.7 V. These two features are due to the sequential depletion of first the top and then the bottom QW, *in the regions directly beneath* the top split gate. Thus, at $V_T \approx -0.7$ V, where electrons beneath the top split gate become completely depleted from *both* QWs, coupled 1D channels are formed in both QWs. Hence this marks the transition from regime (ii), the 1D-2D case, to regime (iii), the 1D-1D case. A simple capacitance calculation predicts the complete depletion of electrons beneath the split gates at $V_T = -0.9$ V, close to the experimental value.

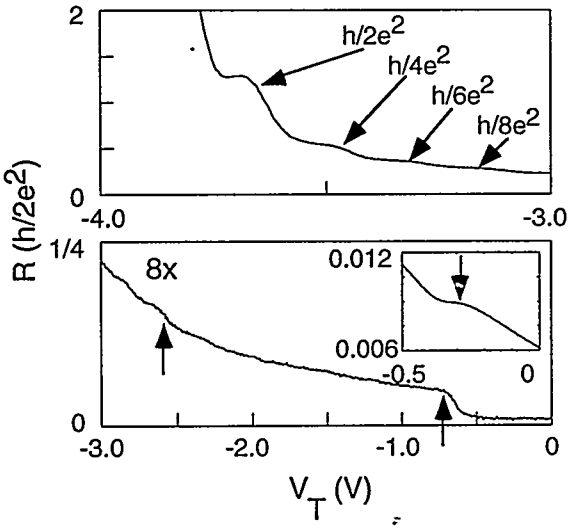


Fig. 2 Resistance of device as $V_T$ is swept with $V_B$ grounded. Inset at bottom shows transition from regime (i) to (ii) at $V_T = -0.3$ V. Transition from (ii) to (iii) can be seen at $V_T = -0.7$ V while distinct increase in slope at $V_T = -2.6$ V marks transition from (iii) to (iv). Bottom figure is magnified 8x to illustrate detail.

As $V_T$ is swept further, we expect the QPC widths to narrow. Due to the fact that the split gate separation is comparable to the electron layer depth, the top channel width narrows more rapidly than the bottom width. At $V_T = -2.6$ V, the top QPC completely pinches off, leaving only the bottom QPC, corresponding to the transition between regimes (iii) and (iv). A weak plateau is observed at this point, as well as a change in the slope of the resistance. As $V_T$ is made yet more negative, the familiar steps in resistance occurring at $h/2ne^2$ ($n = 1, 2, \ldots$) are observed due to the narrowing of the bottom QPC. Finally, at $V_T = -3.8$ V, after the last step at $R = h/2e^2$ occurs, both channels are completely pinched off. Similar results are obtained when instead $V_T = 0$ and $V_B$ is swept negative.

These different regimes are evident in a waterfall plot of the conductance G of the device as a function of both $V_T$ and $V_B$, shown in Fig. 3. Regimes (iii) and (iv) are now easily identified by their markedly different behavior. When only one wire is occupied (regime iv), uniform steps in the conductance quantized in units of $2e^2/h$ appear. This can be seen clearly at the base of the plot, near $V_T = -1.0$ V, $V_B = -2.0$ V, and $V_T = -3.0$ V, $V_B = -1.0$ V. However, when both wires are occupied (regime iii), quantized steps are again present, but form a complicated interference pattern as $V_T$ and $V_B$ are varied. By tracking the position of individual conductance steps as a function of both $V_T$ and $V_B$, each step can be assigned to one quantum wire or the other. As expected, the total conductance of the VCQPC throughout regime (iii) and (iv) agrees with a count of the total number of quantized steps multiplied by $2e^2/h$, indicating that the transport is ballistic. Clearly, each QPC width--and thus the number of occupied

subbands--can be independently controlled by the action of $V_T$ and $V_B$.

We now turn to the behavior of the conductance under an applied magnetic field B perpendicular to both the current and growth directions. Figure 4 shows a contour plot of $\partial[\ln(R)]/\partial V_T$, the logarithmic derivative of the resistance with respect to $V_T$, as a function of $V_T$ and $V_B$, easing identification of the different regimes. Insets (a) – (e) show G vs. B taken at several different values of $V_T$ and $V_B$, as indicated on the main figure by labels. Inset (a) was taken at $V_T$ = -0.25 V and $V_B$ = 0.0 V. The familiar 2D-2D anticrossing features, a conductance peak followed by a shallow dip, are observed centered around B = 6.5 T. This is consistent with the sample being in regime (i). As the sample is biased into regime (ii), the 2D-2D conductance features begin to change. This is evident in inset (b), taken at $V_T$ = -0.50 V and $V_B$ = 0.0 V. Here the 2D-2D conductance features now appear to be superimposed upon a broad conductance dip. For $V_B$= 0 and values of $V_T$ greater than –0.7 V, the 2D-2D conductance features *disappear completely* and are replaced by a *broad conductance minimum* around 6.5 T. This feature is evident in insets (c) and (d), and is a hallmark of conductance behavior in regime (iii). Note that inset (d) is for $V_T$ = -1.75 V and $V_B$ = -1.25 V, showing that this conductance dip occurs over a wide range of $V_T$ and $V_B$, so long as the sample is biased into regime (iii). Eventually, at high enough negative gate bias, the sample moves into regime (iv) where only one QPC remains occupied, and the conductance dip almost completely disappears. This can clearly be seen in inset (e). This phenomenon has been observed in several similar samples, indicating that this broad magnetoconductance dip is a characteristic feature of closely coupled ballistic 1D wires.

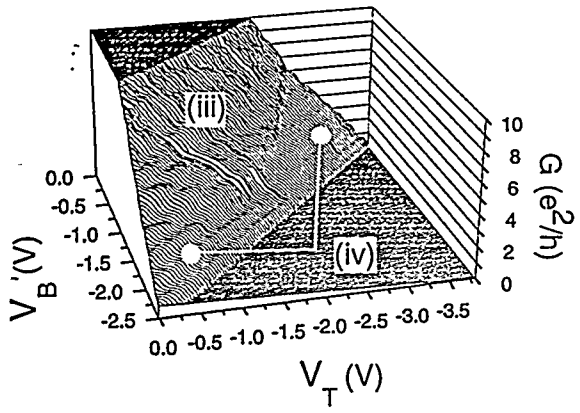


Fig. 3 Waterfall plot of G vs. $V_T$ and $V_B$ shows quantized conductance steps for regime (iv). Beating between steps is evident in regime (iii).

To discuss the origin of this 1D-1D magnetoconductance feature, it is useful to first consider previous work on the 2D-2D case. [4] The 2D-2D magnetoconductance features, exemplified in Fig. 4 inset (a), were shown to arise due to an in-plane magnetic field displacing the two 2D QW dispersion curves relative to each other in k-space by $\Delta k = eBd/\hbar$, where d is the distance between the two electron layers. At sufficiently high B the 2D dispersion curves anticross, forming a partial energy gap. Singularities in the 2D density of states and Fermi velocity occur at the upper and lower gap edges. As B is increased the gap edges cross the Fermi level, producing first a maximum in the conductance, followed by a minimum. These two magnetoconductance anticrossing features are centered about a point $B = [(2\pi n_1)^{1/2} + (2\pi n_2)^{1/2}]h/edB$. Using the measured density values for our sample, we obtain B ≈ 6.5 T, in agreement with the data of Fig. 4 inset (a).

A similar analysis based on the k-space offset of the 1D-1D dispersion curves, combined with the ballistic transport through the sample, explains the 1D-1D data. Due to tunnel coupling, at sufficiently high B the 1D dispersion curves from one wire will anticross with their counterparts from the other wire, opening a quasi gap of $\Delta_{SAS}$, similar to the 2D case. The resulting dispersion curve thus consists of several anticrossed pairs of 1D subbands, as sketched in Fig. 4 inset (f). In our model, we assume that the transport is ballistic and hence the conductance is given simply by the number of 1D subbands crossing the Fermi level. The application of B thus changes the conductance in two ways: (1) Whenever the Fermi level falls within a 1D anticrossing gap, the conductance is reduced by $2e^2/h$ from the uncoupled double quantum wire case. (2) Because for each pair of anticrossed 1D subbands there is a large increase in the density of states at the

edges of the anticrossing gap, each anticrossed pair of subbands can accommodate many more electrons than if no anticrossing occurred. Since particle number is constant, as B is increased and the anticrossings are formed, the Fermi level *drops substantially* and intersects fewer 1D subbands. This results in a large drop in conductance. Eventually B becomes large enough that all the anticrossings in the 1D subbands (and the associated singularities in the DOS) rise above the Fermi level. The number of electrons accommodated by each subband thus correspondingly decreases. As a result, the Fermi level rises again and many more subbands must then become occupied to accommodate all of the electrons, causing the conductance to rise again. While mechanism (1) will only be significant in QPCs with few occupied subbands, mechanism (2) will still be significant for relatively wide QPCs with dozens of occupied subbands.

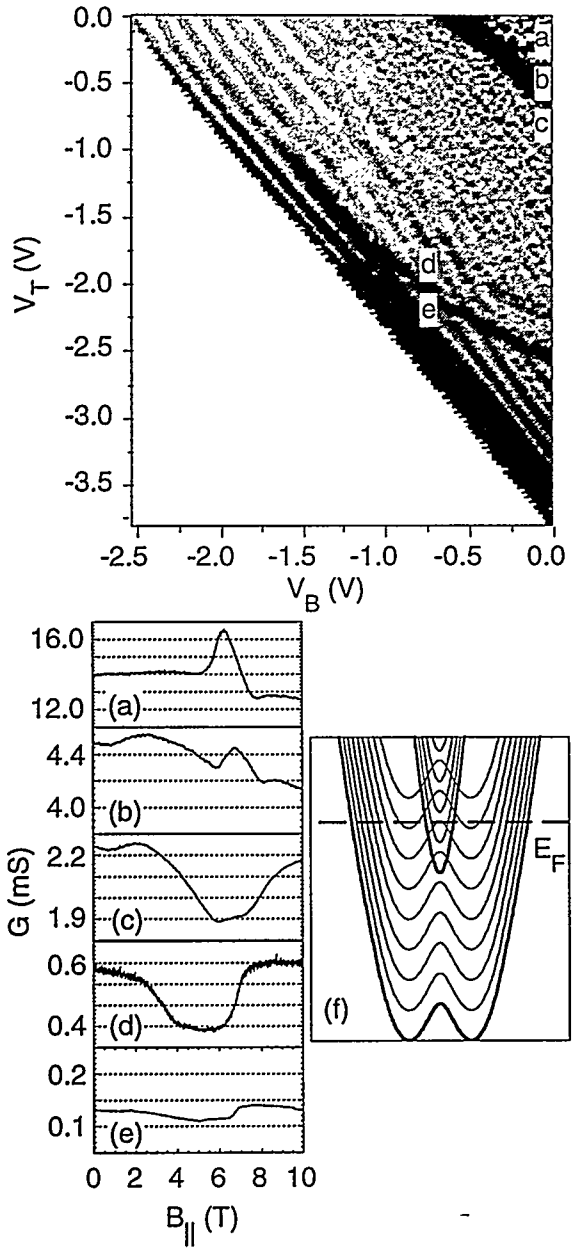


Fig. 4 Contour plot of the logarithmic derivative shows conductance steps in different regimes. Inset s (a) – (e) are magnetoconductance features for the primary regimes of interest. Inset (f) illustrates action of magnetic field on 1-D dispersion curves of VCQPC.

This behavior is consistent with that observed in the data of Fig. 4. The broad magnetoconductance dip appears only when the sample is biased into the 1D-1D regime. Biasing the sample far enough so that only one QPC is occupied extinguishes the magnetoconductance dip, due to the fact that there are no anticrossings present for a single QW. This clearly illustrates that the magnetoconductance dip is present *only when the coupled 1D-1D wires are defined,* i. e. only in regime (iii). This magnetoconductance feature, which is so qualitatively different from that observed in the 2D-2D case, can thus be considered to be an intrinsic property of ballistic transport through closely-coupled QPCs. Our data is consistent with recent theoretical calculations by Lyo. [5]. We note that a similar magnetoconductance dip has been observed by the Nottingham group in a mesa-etched double quantum wire, but was explained using an argument based on diffusive boundary scattering at the wire edges. [2]

Sandia is a multiprogram laboratory operated for the Department of Energy under contract DE-AC04-94AL85000.

[1] Tsukada, *et. al.* Appl. Phys. Lett **56**, 2527 (1990).
[2] Gompertz, *et. al.* Physica B **249**, 162 (1998).
[3] Weckwerth, *et. al.* Superlattices and Microstructures **20**, 561 (1996).
[4] Simmons, *et. al.* Phys. Rev. Lett. **73**, 2256 (1994).
[5] Lyo, to be published.